Received 10 June 2008
Revised 24 November 2008, and 19 April 2009
Accepted 24 April 2009

Simulation of mixed convection in slender rectangular cavity with lattice Boltzmann method

Y. Guo
Dalian University of Technology, Dalian, China, and University of Paris X-Nanterre, Paris, France
R. Bennacer
University of Cergy-Pontoise, Cergy-Pontoise Cedex, Paris, France
S. Shen
Dalian University of Technology, Dalian, China
D.E. Ameziani
University of Cergy-Pontoise, Cergy-Pontoise Cedex, Paris, France, and Université D'Alger, Algiers, Algeria, and
M. Bouzidi
LMSSC, CNAM, IUT, Montluçon, France

Abstract

Purpose – The purpose of this paper is to apply the lattice Boltzmann method (LBM) to simulate mixed flow, which combines natural convection for temperature difference and forced convection for lid driven, in a two-dimensional rectangular cavity over a wide range of aspect ratios (A), Rayleigh numbers (Ra) and Reynolds numbers (Re).

Design/methodology/approach – The LBM is applied to simulate the mixed flow. A multi-relaxation technique was used successfully. A scale order analysis helped the understanding and predicting the overall heat transfer.

Findings – In the considered lid driven cavity, the Richardson number emerges as a measure of relative importance of natural and forced convection modes on the heat transfer. An expression of the overall heat transfer depending on the cavity slender (A) is deduced. The validity of the obtained expression was checked in mixed convection under the condition of low Richardson number (Ri) and the limitation condition was deduced.

Practical implications – This paper has implications for cooling system optimization and LBM technique development.

Originality/value – This paper presents a new cooling configuration, avoiding critical situation where the opposing effect induce weak heat transfer; and a stable and fast LBM approach allowing complex geometry treatment.

Keywords Simulation, Convection, Flow, Temperature distribution

Paper type Research paper

1. Introduction

In recent years lattice Boltzmann method (LBM) draws more and more attention for it has a simple program, it is easy to treat complex boundary condition and it is suitable for parallel calculation. This method is based on a microscopic model but is used to model macroscopic fluid properties such as density, velocity and temperature. That is why sometimes it is called a mesoscopic method. The fundamental idea of LBM is to describe a fluid as an ensemble of many particles interacting locally at the nodes of a regular lattice by collisions, and then the particles move only along the lattice and collide again with other particles once they arrive at the nodes. During the movement, the quality, the momentum and the energy are transported. This discrete microscopic

International Journal of Numerical Methods for Heat & Fluid Flow
Vol. 20 No. 1, 2010
pp. 130-148

0961-5539
DOI 10.1108/09615531011008163

model can be shown to recover the conservation laws of continuum fluid dynamics, and, thus, allows the calculation of the macroscopic variables such as density and velocity. It could be used for dealing with phase separation (Xu *et al.*, 2003; Vladimirova *et al.*, 1999; Suppa *et al.*, 2002), diffusion (Shan and Doolen, 1995), wetting (Raiskinmäki *et al.*, 2000; Iwahara *et al.*, 2003), evaporation (Palmer and Rector, 2000), particle-fluid suspensions (Ladd, 1994), flow in porous media (Succi *et al.*, 1989; Heijs and Lowe, 1995) and heat transfer (Alexander *et al.*, 1993; He *et al.*, 1998; Tang *et al.*, 2003). There are mainly three LBM models for heat transfer simulation: multi-speed model (McNamara and Alder, 1993; Alexander *et al.*, 1993; Chen *et al.*, 1994), double-distribution function model (He *et al.*, 1998) and finite-difference model (Zhang and Chen, 2003; Mezrhab *et al.*, 2004). Finite-difference model is known as hybrid LB finite-difference method, where the temperatures are obtained by solving discrete macro-energy equation with finite-difference method, during which the velocity calculated by LBM is needed. In multi-speed model, the internal energy is involved in the density distribution function, and the temperature can be expressed with the distribution function just as velocity. This model has a poor stability. Different from this model, in double-distribution function model, besides the density distribution function there is another distribution function known as the energy distribution function, based on which the internal energy equation evolution can be developed. The form of the energy distribution function is same as that of density distribution except that it is scalar quality while the latter is vector. In this work, we adapt the double-distribution model. To reduce the calculation time, a simpler model *D2Q5* is applied to simulate temperature while *D2Q9* is for velocity simulation (Ameziani *et al.*, 2008).

The lid driven cavity flow is widely studied with macro-methods for the complexity of this flow and *LB* models are often tested and evaluated on this flow (Hou *et al.*, 1995; Guo *et al.*, 2000; Chew *et al.*, 2002; Haibo Huang *et al.*, 2007). It is a model for flow in a cavity where the upper boundary moves to the right, and thus causes a rotation in the cavity. When there is temperature difference, the complexity of cavity flow is intensified, because more forces act on the fluid flow such as buoyancy, mass force and viscous force if viscosity is considered. A lot of experiments and numerical simulations on the two-dimensional flow in a cavity have been conducted. However, few published articles on lid driven cavity flow with heat transfer are found in case of vertical applied temperature gradient (Wong, 2007) and relatively little investigation has been carried out for flow in the rectangular cavity where aspect ratio is not 1 (Patil *et al.*, 2006; Cheng and Hung, 2006). Only some are about the vortices investigated at different Reynolds number. Also there are no analysis on interaction between fluid flow and heat transfer and to our knowledge no work deals with the present case where the driven cavity is parallel to the temperature gradient. Generally, in rectangular cavity, especial deep cavity, owing to the slow penetration of the field into the depths and the large number of grid points required, it is difficult to make accurate calculations without an efficient numerical method. Just as been pointed out by Shankar and Deshpande (2000), numerical computations can be difficult even for Stokes flow for deep cavities. At un-adiabatic condition, buoyancy led by temperature difference would affect the flow, and the velocity of flow in reverse would work on the process of heat transfer. That further intensifies the difficulties. There lacks of a numerical description on such effect.

In this work a mix convection flow combining natural convection motivated by buoyancy formed, because of horizontal temperature difference, and lid driven forced convection is simulated with LBM in rectangular cavity with different aspect ratios.

The heat transfer ability is investigated at different Rayleigh numbers, Reynolds number and aspect ratios. By normalizing the average Nusselt number, generalized formulas are obtained based on the value of Richardson number, according to which the dominant flow (natural convection dominant or forced convection dominant) can be identified. The effect of aspect ratio on the transition point of Richardson number, where the mixed flow changes to forced convection dominant, is analyzed. The *LB* moment model is introduced in the next section and the results are compared with benchmark, a good agreement is obtained. In the third section, the physical goal to be studied is presented and the simulation results are obtained with the *LB* moment model. The conclusion is made in the last section.

2. Lattice Boltzmann method

Density simulation

Let us follow the usual nomenclature and indicate the LB models as D*I*Q*J*, where $I = 2$, 3 is the spatial dimension and J is the number of discrete velocities.

In this section, we will present the *D2Q9* (two dimension, nine discrete velocities, see Figure 1) moment model (Mezrhab *et al.*, 2004, 2007; Tekitek *et al.*, 2006;) used to compute the velocity and the temperature.

The particles distribution Boltzmann equation is expressed as

$$\frac{\partial \vec{f}}{\partial t} + \vec{c}\,\nabla\vec{f} = \left(\frac{\partial \vec{f}}{\partial t}\right)_{scat} \tag{1}$$

where, f(x, c, t) is the distribution function, which is function of particle velocity c at location x and at time t. The subscript "scat" means scatter and the term on the right hand in equation (1) represents the diffusion process when the new equilibrium distribution is rebuilt after the collision. In general, this term is non-linear and there are different methods to treat it. Based on *D2Q9* model, where the state of the fluid at location **r** and time t is defined as $F(r,t) = \{f_0(r,t), f_1(r,t), \ldots, f_8(r,t)\}$ with a vector

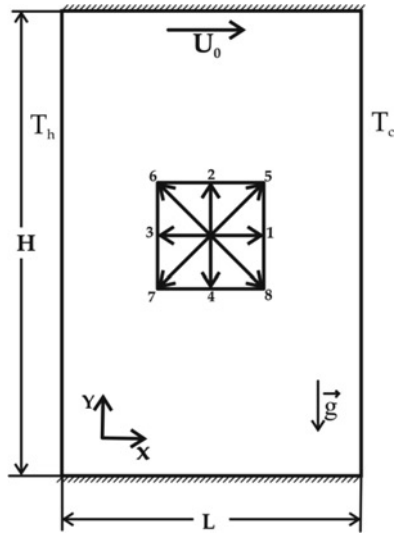

Figure 1.
Geometrical configuration

of particles populations f_i ($i = 0, 1, \ldots, 8.$, the discrete distribution equation is as follows:

$$f_i(x + c_i, t + 1) = f_i(x, t) + (\Omega F)_i \tag{2}$$

where, the micro-discrete velocities c_i are, respectively, equal to 0 ($i = 0$), 1 (for $i = 1$ to 4), and $\sqrt{2}$ (for $i = 5$ to 8), where i refers to the discrete velocity direction. F is the vector space based on the discrete velocity set. Ω is the collision operator, it can be represented in different formula based on different approximation and one of the method would be introduced later.

One can interpret the dynamics of the model as a succession of two steps: propagation of particles from nodes to their neighbors and collision or redistribution between the various velocities c_i at each lattice node. In the present study, the *D2Q9* model adapted combines the vector space and the moment space. That is, as mentioned above, the state of the fluid at location x and time t is defined with a vector of 9 dimensions so that a $N \times 9$-dimensional vector space $F = R^{9N}$ could be constructed based on the discrete velocity set $\{c_i\}$, where N is the space node number. At the same time, a space $M = R^{9N}$ could also be constructed based on the moments of $\{f_i\}$. Obviously, there are 9 independent moments for the discrete velocity set at each lattice nodes. One should notice that in real space F it is easy to handle the propagation step of the evolution in equation (2), whereas it is preferably to treat the collision part of the equation in M space (Mezrhab *et al.*, 2007). The relationship between the two spaces is as expressed by d'Humieres (1992):

$$m_j = \sum_i a_{ij} f_i \tag{3}$$

where the coefficients a_{ij} are constructed from the velocities c_i, and must not be singular as the following:

$$[a_{ij}] = \begin{pmatrix} 1 & 1 & 1 & 1 & 1 & 1 & 1 & 1 & 1 \\ 0 & 1 & 0 & -1 & 0 & 1 & -1 & -1 & 1 \\ 0 & 0 & 1 & 0 & -1 & 1 & 1 & -1 & -1 \\ -4 & -1 & -1 & -1 & -1 & 2 & 2 & 2 & 2 \\ 0 & 1 & -1 & 1 & -1 & 0 & 0 & 0 & 0 \\ 0 & 0 & 0 & 0 & 0 & 1 & -1 & 1 & -1 \\ 0 & -2 & 0 & 2 & 0 & 1 & -1 & -1 & 1 \\ 0 & 0 & -2 & 0 & 2 & 1 & 1 & -1 & -1 \\ 4 & -2 & -2 & -2 & -2 & 1 & 1 & 1 & 1 \end{pmatrix} \begin{matrix} \rho \\ j_x \\ j_y \\ E \\ T_{xx} \\ T_{xy} \\ \phi_x \\ \phi_y \\ \varepsilon \end{matrix} \tag{4}$$

where the signals on the right line beside the matrix are corresponding to the physical modes calculated from every row based on formula (3). That is to say, the first row in the matrix allows to compute the density ρ; the second and third rows are for the x and y components of momentum (mass flux) j_x and j_y. E is related to the kinetic energy. T_{xx} and T_{xy} correspond to the diagonal and off-diagonal components of the stress tensor. ϕ_x and ϕ_y are the x and y components of the energy flux, ε is related to the square of the energy.

Now it comes to define the collision operator Ω. It is known that the collision step would not modify the moments such as mass, energy and linear momentum if there is

no body force. Therefore, these conserved moments satisfy the following relations:

$$m_0^{ac} = m_0^{bc} = \rho \tag{5}$$

$$m_1^{ac} = m_1^{bc} = j_x \tag{6}$$

$$m_2^{ac} = m_2^{bc} = j_y \tag{7}$$

where m_j^{ac} and m_j^{bc} are the moments after collision and before collision, respectively. For the non-conserved moments, the collision and relaxation process can be expressed as

$$m_j^{ac} = m_j^{bc} + s_j(m_j^{eq} - m_j^{bc}) \tag{8}$$

where s_j is a relaxation rate. To have numerical stability, it is necessary to take the relaxation rates between 0 and 2 (Mezrhab *et al.*, 2004). And m_j^{eq} is the value of moment j when the system reaches equilibrium.

Though the local energy conservation is destroyed by collision, the total energy is conserved. The values of moments when the system is at equilibrium are (Shankar and Deshpande, 2000):

$$m_3^{eq} = (6c_s^2 - 4)\rho + 3\frac{j_x^2 + j_y^2}{\rho} \tag{9}$$

$$m_4^{eq} = \frac{j_x^2 - j_y^2}{\rho} \tag{10}$$

$$m_5^{eq} = \frac{j_x j_y}{\rho} \tag{11}$$

$$m_6^{eq} = -j_x \tag{12}$$

$$m_7^{eq} = -j_y \tag{13}$$

$$m_8^{eq} = \rho - 3\frac{j_x^2 + j_y^2}{\rho} \tag{14}$$

This model behaves as a viscous fluid with speed of sound $c_s = 1/\sqrt{3}$ and kinematics shear viscosity $\upsilon = 1/3[(1/s_4) - (1/2)]$. Second-order results could be obtained with this model.

Compared with the classical *LBGK* model, this *LBE*-moment model has a higher stability. It allows reducing the influence of compressibility effects and a large bulk viscosity is used in situations where a small shear viscosity is needed. In addition, in most cases the variations of the density are small, therefore the ρ appearing in the formulas from (9) to (14) could be replaced by ρ_0 and be forgotten when it is at the denominators. This not only saves computational time but more important it permits to work when the mean calculation density is 0.

Temperature simulation

The double distribution functions are adapted to simulate the temperature. A same moment model is applied except that the first moment described in last session to calculate density turns to calculate temperature and the collision and relaxation step

becomes related to node velocity obtained by last session. Therefore, the interaction of velocity and temperature is realized in computational way. To save the calculation time, a *D2Q5* model is used for energy equation instead of the *D2Q9* model. The flow is well resolved by the *D2Q9* and as the energy is scalar transport we used the *D2Q5* to reduce the computing time. With such approach, the energy resolution needs half time compared to that with the *D2Q9*. The simulation results expressed later would show that this simplifying method is effective.

Because of temperature difference between the two vertical walls, the buoyancy force $\boldsymbol{f} = \mathrm{a} \times \mathrm{T}(\mathrm{x}, \mathrm{t})$ is produced in the y direction. Where $\mathrm{a} = \mathrm{g}\ \beta$, and it plays the role of $\mathrm{g}\beta$ in a real fluid, g being the acceleration due to gravity and β being the thermal expansion coefficient. The buoyancy is acting as body force and modifies the conservation of linear momentum in the collisions. Thus the formulas (6) and (7) turn to:

$$\mathrm{m}_1^{\mathrm{ac}} = \mathrm{m}_1^{\mathrm{bc}} + \boldsymbol{f}_{\mathrm{x}} \tag{15}$$

$$\mathrm{m}_2^{\mathrm{ac}} = \mathrm{m}_2^{\mathrm{bc}} + \boldsymbol{f}_{\mathrm{y}} \tag{16}$$

where $\boldsymbol{f}_{\mathrm{x}}$ and $\boldsymbol{f}_{\mathrm{y}}$ are, respectively, the x and y components of the body force. Obviously, in view of simulation method, the temperature and velocity are associated.

The present mixed convection considered problem fit with the classical natural convection problem for the zero lid driven velocity ($\mathrm{U}_0 = 0$) and fit with the lid driven cavity when the buoyancy forces are nil ($\boldsymbol{f}_{\mathrm{x}} = \boldsymbol{f}_{\mathrm{y}} = 0$).

In this work, the viscous fluid flow with Prandtl number 0.71 is investigated in a rectangular cavity. The aspect ratio, $A = \mathrm{H/L}$, varies from 1.0 to 7, where H and L are, respectively, the rectangular height and width. As shown in Figure 1, the present simulation uses Cartesian coordinates with the origin located at lower left corner. The left and right walls are maintained at constant and different temperature (hot and cold, respectively). The upper and bottom surfaces were assigned to adiabatic boundary conditions. The top surface moves horizontally from left to right in its own plane. Initially the velocities at all nodes, except the top nodes, are set to zero. The top surface x-velocity component is U_0 and the y-velocity is zero. Boundary condition commonly used at solid wall is the no-slip condition for which the relative velocity of the fluid with respect to the wall vanishes. This is implemented in the LBM with the bounce-back rule in which all particles hitting the wall are reflected back in the direction of the source.

The temperature boundary conditions are set between two consecutive nodes as:

$$\begin{aligned}
&\text{Left boundary}: \theta(1/2, \mathrm{y}) = \theta_{\mathrm{h}} = 0.5 && (1/2 \le \mathrm{y} \le \mathrm{N_y} + 1/2)\\
&\text{Right boundary}: \theta(\mathrm{N_x} + 1/2, \mathrm{y}) = \theta_{\mathrm{c}} = -0.5 && (1/2 \le \mathrm{y} \le \mathrm{N_y} + 1/2)\\
&\text{Bottom boundary}: (\partial\theta/\partial\mathrm{y})(\mathrm{x}, 1/2) = 0 && (1/2 \le \mathrm{x} \le \mathrm{N_x} + 1/2)\\
&\text{Top boundary}: (\partial\theta/\partial\mathrm{y})(\mathrm{x}, \mathrm{N_y} + 1/2) = 0 && (1/2 \le \mathrm{x} \le \mathrm{N_x} + 1/2)
\end{aligned}$$

where θ is the dimensionless temperature, and the subscripts *h* and *c* are, respectively, hot and cold temperature. $\mathrm{N_x}$ and $\mathrm{N_y}$ are the lattice numbers in x and y direction, respectively, and they satisfy $\mathrm{N_y} = A\ \mathrm{N_x}$.

The velocity boundary conditions are:

Top boundary: $v_x(x, N_y + 1/2) = U_0, v_y(x, N_y + 1/2) = 0\ (1/2 \leq x \leq N_x + 1/2)$, and zero for the other velocity boundaries. Where, $\mathbf{v_x}$ and $\mathbf{v_y}$ are the velocities in x and y direction, respectively.

So before analyzing the coupled problem, we present in the next section our code validation in the two extreme situations, i.e. natural convection and lid driven cavity.

Validation of the LB moment model

As the present work deals with the natural convection coupled to the lid driven cavity we will present the numerical validation in the two separate phenomena, i.e. natural convection followed by the lid driven cavity. The present LB moment model was validated by considering the first case of natural convection in a 2D square cavity. In the simulation, the square cavity was assumed to be closed and the no-slip boundary condition was applied to the four solid walls ($U_0 = 0$, $\theta_{left} = \theta_h = 0.5$ and $\theta_{right} = \theta_c = -0.5$). The considered fluid is the air, so the Prandtl number was fixed at a value of 0.71. Table I presents the Nusselt number obtained in the present work and those of some other reference (Semma *et al.*, 2008; Choukairy *et al.*, 2004; Sai *et al.*, 1994; De Vahl Davis and Jones, 1983) for a wide range of Rayleigh number, $Ra = 10^3$ to 10^6. It is obvious from this table that there are good agreements between the present results and the obtained by other authors.

The second case considered for the validation, as previously underlined, concerns the lid driven cavity. The flow simulations are carried out at different Reynolds numbers, i.e. velocity U_0. Figure 2 shows the velocity components $\mathbf{v_x}$ and $\mathbf{v_y}$ along the mid-sections in the x- and y-directions for $Re = 10^3$ and 5×10^3. The results closely agree with the Navier-Stokes (*N-S*) results of in literature (Ghia *et al.*, 1982). The streamlines are plotted in Figure 3 for these two Reynolds numbers. It is clearly seen that compared with $Re = 10^3$, the increases of Re to 5×10^3, a new secondary vortex is visible at the left upper corner besides the main vortex in the center of the cavity and the two secondary vortex at left and right bottom corners, and a third class vortex emerges at the right bottom corner. The agreement is good with the previously established benchmark (Ghia *et al.*, 1982). The simulations are carried over a large domain of Re from 1 to 2,000 and good agreements are found (but not presented due to lack of space). Therefore, the present model can be applied to simulate the coupled forced and natural convection in the present considered domain.

3. Mixed flow in rectangular cavity

The mixed flow in rectangular cavity is simulated for wide range of aspect ratio, $A \in [1, 7]$, Reynolds number, $Re \in [0, 2 \times 10^3]$ and Rayleigh number, $Ra \in [10^0, 5 \times 10^6]$. Series of simulations have been done and the results are obtained at different conditions. A time independent problem is considered in the simulations.

Table I. Comparison of Nusselt numbers at different Rayleigh numbers with some existing works

Authors	$Ra = 10^3$	10^4	10^5	10^6
Semma *et al.* (2008)	1.116	2.245	4.521	8.814
Choukairy *et al.* (2004)	1.117	2.241	4.513	–
Sai *et al.* (1994)	1.130	2.289	4.687	–
De Vahl Davis and Jones (1983)	1.117	2.238	4.509	8.817
Present LB moment model	*1.117*	*2.242*	*4.517*	*8.813*

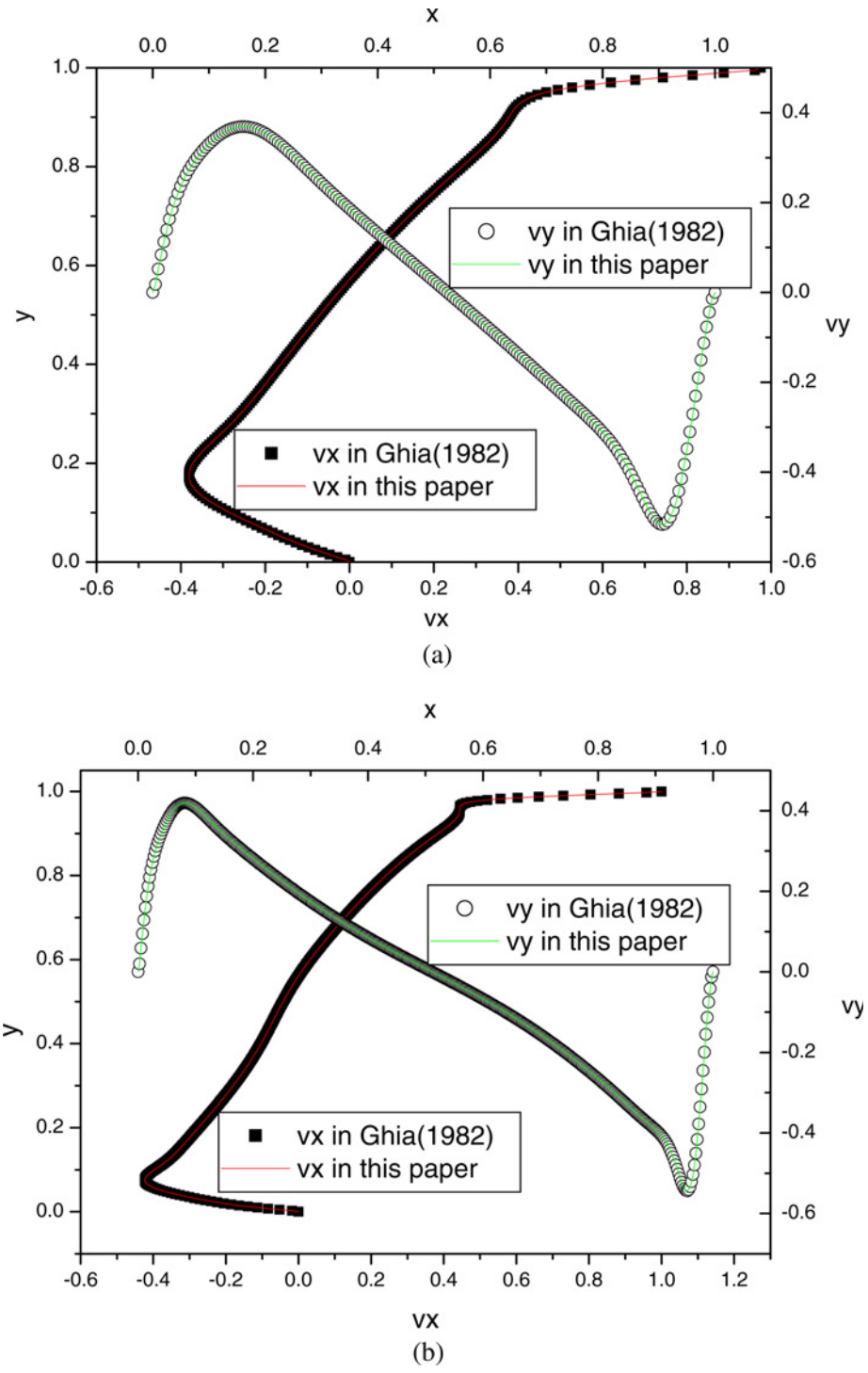

Figure 2.
The x and y velocity components on the vertical and horizontal mid-planes for $Re = 10^3$ (a) and $Re = 5 \times 10^3$ (b)

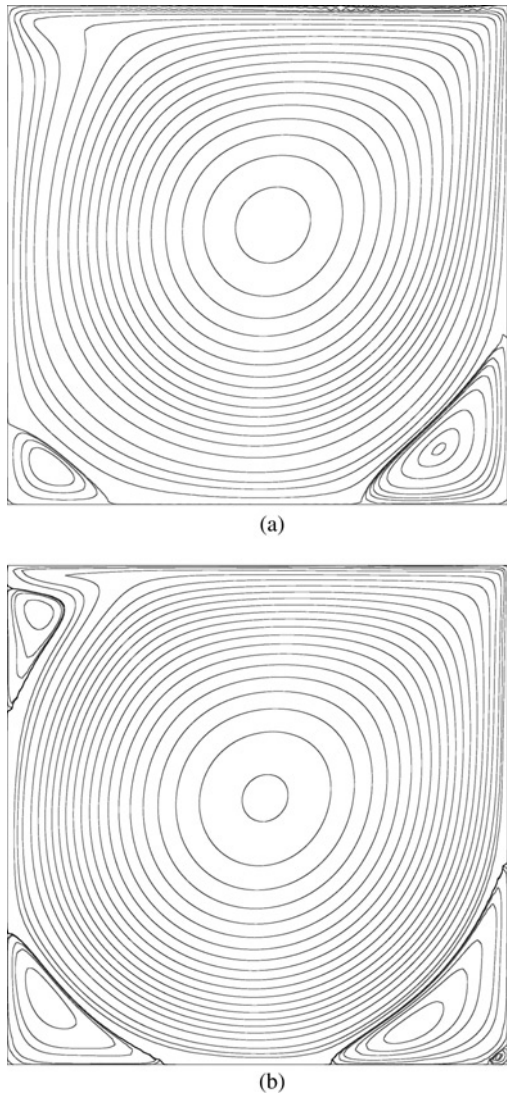

Figure 3.
Streamlines of lid driven square cavity for $Re = 10^3$ (a) and $Re = 5 \times 10^3$ (b)

To have a primary opinion about flow and heat transfer in a slender rectangular, the aspect ratio equal to two is first studied and typical results of the isotherms and streamlines for different Re and Ra are shown in Figures 4 and 5. We will discuss the effect of natural convection on the flow structure and the corresponding heat exchange at different applied forced convection (Re values). The results reveals, for moderate Re, $Re = 100$, that the flow topology consists of one main cell on the top of the cavity (noted *C1*) and secondary cell on the lower part (*C2*) for weak buoyancy forces ($Ra = 1$). The resulting flow is mainly due to the imposed lid driven condition. The main *C1* induce an over pressure in the vicinity of the top right corner and pressure drop near the left top corner. The resulting flow from left to right near the top induces a fluid recirculation toward the left in the clockwise direction. The obtained *C1* do not fill

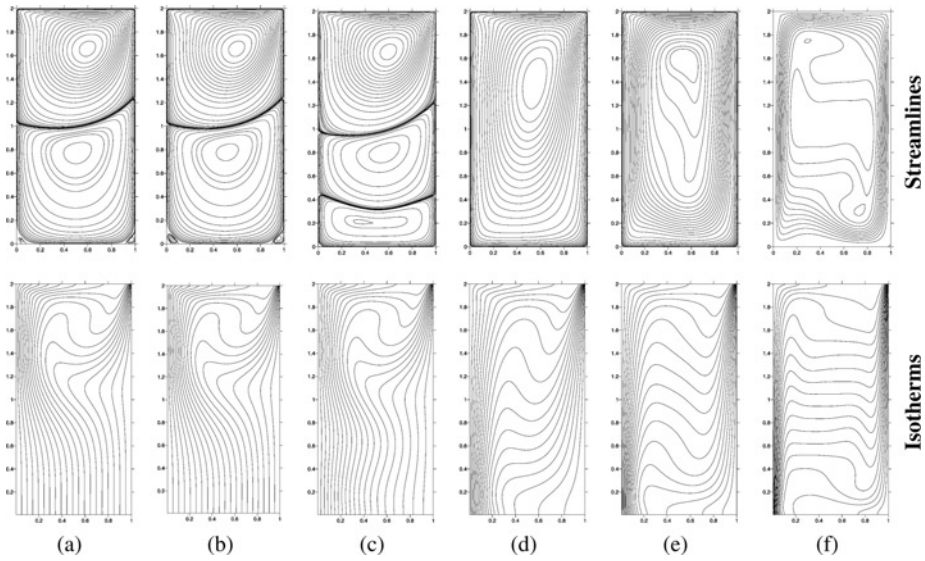

Figure 4.
Streamlines (upper) and isotherms (bottom) at different Rayleigh numbers Ra = 10^0 (a), 10^2 (b), 10^3 (c), 10^5(d), 5×10^5, (e) and 5×10^6 (f) (for Re = 10^2)

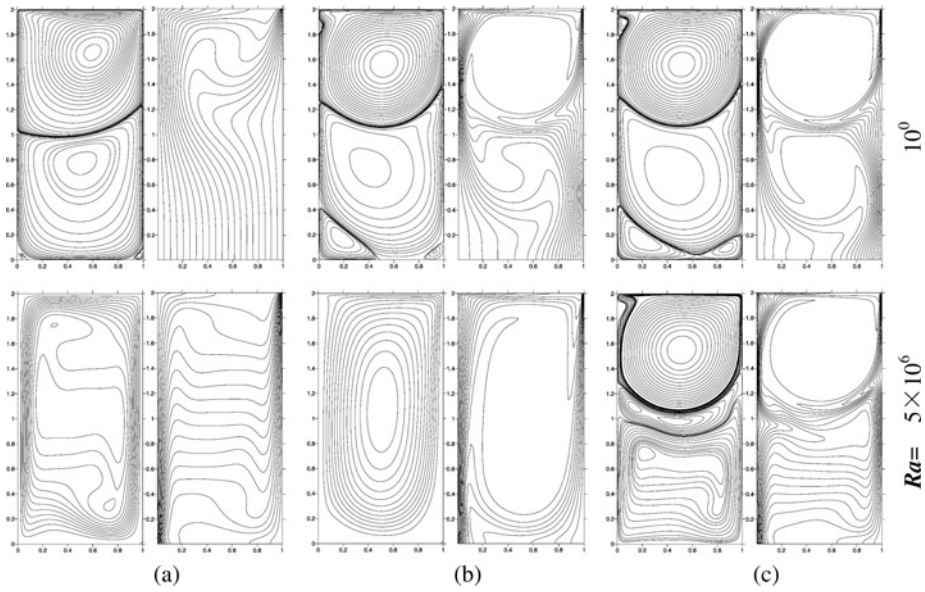

Figure 5.
Streamlines (left) and isotherms (right) at different Reynolds numbers, Re = 10^2 (a), 10^3 (b) and 2×10^2 (c) (for Ra= 10^0 and 5×10^6)

the entire domain because of the underlined pressure gradient. So the obtained *C1* fit a relative square domain. The observed secondary *C2* is a direct consequence of the shear stress. We mention two corner small vortices (*C3*) at the bottom corners.

It is obvious from the corresponding temperature field that:

- the transfer is convective in the upper part of the domain illustrated by the classical vertical temperature stratification in the bulk of the cell;

- the transfer is conductive in the lower part where the parallel and linear characteristic temperature profile is from the hot to the cold surface.

The thermal resulting buoyancy forces tend to induce a flow in the clockwise direction. So it induces a cooperative effect on the *C1* and *C3* and opposing effect on *C2*.

When Rayleigh number increases (Figure 4c), there is a coalescence of the two corner vortices (*C3*) together, giving rise to a third primary-eddy. The *C2* intensity and shape decrease as consequence of the opposing effect.

A dynamic competition occurs between the natural and forced convection effect. So a complex flow remains for Ra below a critical value. Above this value the buoyancy forces overcome the lid driven imposed flow and a main cell takes place and covers the entire domain (Figure 4d). For high Ra values the flow becomes mainly due to the natural convection effect (Figure 4f) which is also obvious from the temperature field. Such main convective cell (for $\mathrm{Re} = 100$) is obtained for Ra values above 10^5. However such identified value is of the applied Re number. In order to illustrate such effect we present in Figure 5 the Re effect for two Ra values (low $\mathrm{Ra} = 1$ and high $\mathrm{Ra} = 5 \times 10^6$) to illustrate the competition between the imposed natural and forced convection.

It is obvious from this figure that the flow,

- for $\mathrm{Re} = 10^2$, it passes from forced dominating case (low Ra, multicells) to natural dominating effect for $\mathrm{Ra} = 5 \times 10^6$, with one main cell thermally stratified;
- for $\mathrm{Re} = 10^3$, it passes from forced dominating case (low Ra) to one main cell effect for $\mathrm{Ra} = 5 \times 10^6$. Nevertheless, the thermal field exhibits that it is not yet natural convection dominating and the two effect are cooperating and of the same order of magnitude;
- for high $\mathrm{Re} = 2 \times 10^3$, the multicells remain for the two presented Ra. For low Ra it is the forced dominating case. And for $\mathrm{Ra} = 5 \times 10^6$, the upper *C1* cell is still mainly imposed by the driven effect (forced) and in the lower part it is a natural convection cell (*C3*). As the two cells are rotating clockwise it remains a third cell (counter clockwise) in order to minimize the shear stress between these two main cells. The thermal field analysis illustrate that the previously underlined diffusive field (in low Ra case) in the bottom part becomes a convective with the Re increase. Such convective effect is a consequence of the important drag effect inducing a strong re-circulating flow in the lower half part.

As the present problem exhibits a competition between the natural and forced convection we use the classical Richardson number (Ri) to define when one of the two phenomena is dominating (see for instance Wong, 2007).

$$\mathrm{Ri} = \frac{\mathrm{Ra}}{(\mathrm{Pr} \cdot \mathrm{Re}^2)}$$

When it is kept constant, the Richardson number can be thought as the ratio of the natural convection effect to that of forced convection. If the Richardson number is much less than unity, the buoyancy is unimportant in the flow. If it is much greater than unity, the buoyancy is dominant (in the sense that there is insufficient kinetic energy to homogenize the fluids). If the Richardson number is of order unity, then the flow is likely to be buoyancy-potential energy (the energy of the flow derives from the

potential energy in the system originally) driven. This confirms the previous remarks concerning the obtained flows (Figures 4 and 5) dominated by the natural or forced convection.

To investigate how Rayleigh number and Reynolds number modify the resulting heat transfer we plot the normalized average Nusselt number Nu_n (the forced convection Nusselt number Nu_{fc} is considered as reference case) vs the Richardson in Figure 6 (for A = 2).

On the whole, Figure 6 is made up of three parts: a horizontal line representing the forced convection dominant flow where the average Nusselt number only changes with Reynolds number and is represented by Nu_{fc}, a declining line on right representing the natural convection dominant flow where only Rayleigh number affects the average Nusselt number represented by Nu_{nc} and the middle part composing by some discrete points representing the mixed flow. It can be observed that when Ri is lower than 0.1, the flow is dominated by forced convection where the flow does not affected by the value of Rayleigh number. The Nusselt number Nu changes with Re in this domain as

$$Nu_{fc} = 0.616 \times Re^{0.47} \tag{17a}$$

If Ri reaches above 10, natural convection would govern the flow, the relationship between the parameters can be expressed as

$$Nu_{nc} = 0.603 \times Ra^{0.21} \tag{17b}$$

That reveals the average Nu only affected by Ra. When Ri is located between 0.1 and 10, the flow exhibits a typical mixed flow, where natural convection and forced convection play the same important roles on fluid flow and the obtained heat transfer

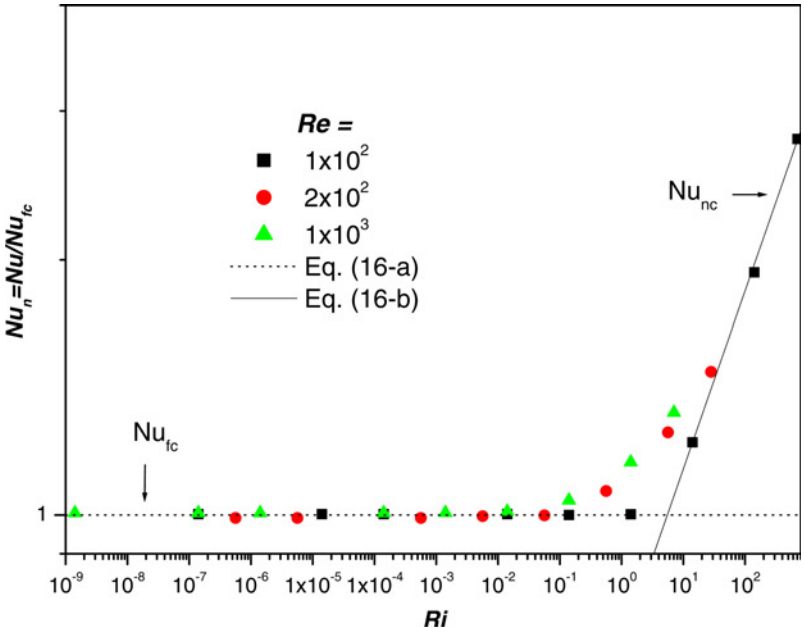

Figure 6.
Normalized average Nusselt number (Nu_n) vs Richardson number (Ri)

include the two contribution. We have verified the cases of A = 3, 4, 5, 6, 7 and equations (17a) and (17b) still hold.

Therefore, for low Reynolds number the whole domain tends to be natural convection dominated when Rayleigh number is not as large as that for high Reynolds number. For higher Reynolds number, the velocity shear by the lid is much sufficient to overcome the tendency of the stationary fluid to remain stationary, therefore, the series of successive, counter-rotating vortices are formed in the whole rectangular and the bottom corner is larger than that when Reynolds number is smaller. With the increase of Rayleigh number, the two bottom corner vortices coalesce together and giving rise to a third primary-eddy. When the value of Ri is kept in the order of unity (typically shown in Figures 5 when Re = 2,000 and $Ra = 5 \times 10^6$), the flow is affected by both energy from driven lid and the buoyancy. The upper domain is mainly force flow while the bottom third eddy is dominated by natural convection rather than forced convection. As the consequence, the middle vortices turn less and less and the bottom eddies larger and larger when Rayleigh number increases.

After Ri goes beyond the order of unity (typically in Figure 5 when Re = 100 and $Ra = 5 \times 10^6$), the flow is dominated by natural convection. The streamlines show a clockwise rotating cell fills up the entire cavity with hydrodynamic boundary layers along the vertical walls and a motionless core region. The temperature field indicates the existence of thermal boundary layers along the vertical isothermal walls, the temperature variation being large in these boundary regions. It is noticed that, for lower Reynolds number, the temperature in the core of the cavity is nearly constant in the horizontal direction and varies almost linearly in the vertical direction (see Figure 5 when Re = 100 and $Ra = 5 \times 10^6$).

No doubt that the previously discussed competition depends on the aspect ratio especially because the forced convection main cell has a square shape (for the considered Pr number). So it will occupy less space with A increase. Now it goes to the effect of the domain aspect ratio on fluid flow and heat transfer. The local Nusselt number on the right cold wall for different aspect ratios is shown in Figure 7 (for Ra = 1 and Re = 100). Obviously it can be observed that each curve consists of two parts: curved region and vertical region. The vertical regions of the curves in this figure, where the local Nusselt numbers do not change with the cavity height, represent the lower conduction heat transfer region in the rectangular. It can be seen that the local Nusselt value is equal to A, with the present considered dimensionless. In this region, Nusselt number is independent of Reynolds number and only changes with A because the convective cell is located on the upper part of the domain. Above the previous vertical area the forced convection flow fields will modify significantly the temperature and the flow intensity directly and local Nusselt number is related to the Reynolds number.

A flow and temperature fields for two A (A = 3 and 5) are represented in Figure 8 where it confirms the two distinct domains corresponding to the lower conductive part increasing with A and the upper convective cell with a relative square shape.

The height occupied by every region in the vertical direction is directly related to the aspect ratio. It is clear that the main vortex in the rectangular occupies about 1/3 height of the rectangular for A = 3 and about 1/5 height of it for A = 5. That is, the main forced convection vortex region occupies about 1/A height of the rectangular. Therefore, we can conclude that the total average Nusselt number should be composed by convection and conduction contributions, and be expressed as

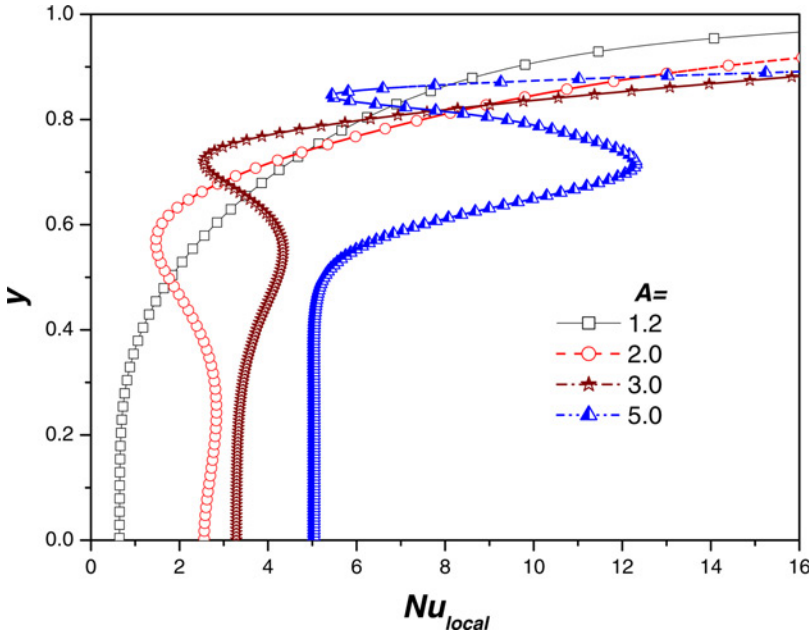

Figure 7.
Local Nusselt number on the vertical wall for different aspect ratio, A (Ra = 1 and Re = 100)

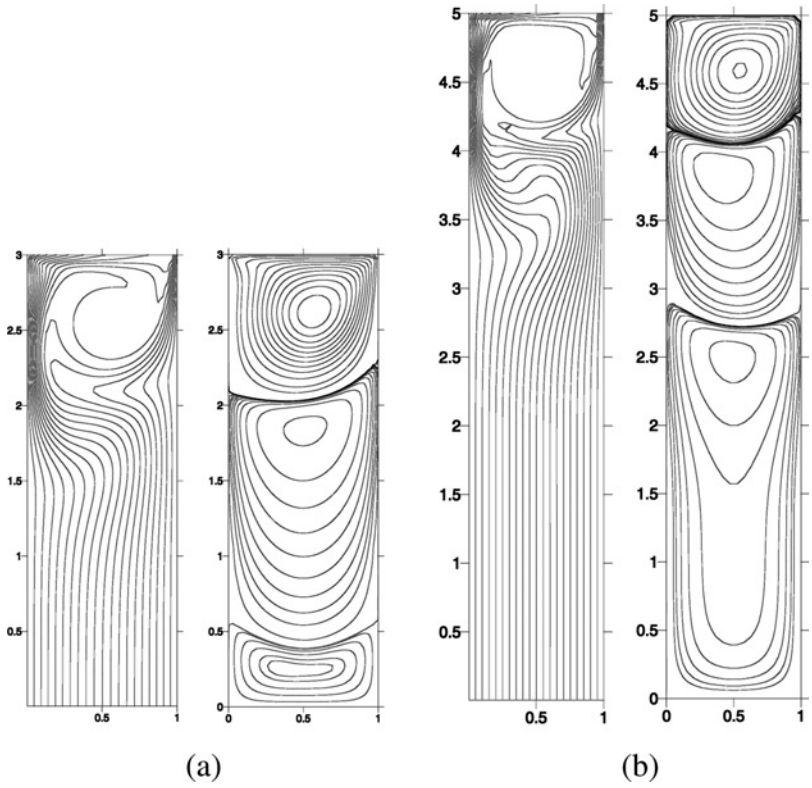

Figure 8.
Isotherms and streamlines for A = 3 (a) and A = 5 (b) (for Ra = 1 and Re = 100)

$$\mathrm{Nu} = \mathrm{Nu_{cv}} \times \frac{1}{\mathrm{A}} + \mathrm{Nu_{cd}} \times \left(1 - \frac{1}{\mathrm{A}}\right) \tag{18}$$

where $\mathrm{Nu_{cv}}$ and $\mathrm{Nu_{cd}}$, respectively, represent the Nusselt number for the upper convective region and the lower conductive region. We have tested another cases of $\mathrm{Ra} = 1$ and $\mathrm{Re} = 10, 20, 50$ and the same relationship as described in equation (18) is obtained. Distinctly it could be confirmed from what mentioned above that

$$\mathrm{Nu_{cd}} = \mathrm{A} \tag{19}$$

The $\mathrm{Nu_{cv}}$ changes with the relative parameters is defined based on our test as

$$\mathrm{Nu_{cv}} = 0.254 \times \mathrm{Re}^{0.47}\mathrm{A}^{3/2} \tag{20}$$

The observed A effect is a direct consequence of the dynamic boundary layer development along the lid driven surfaces and the competition between the horizontal energy transport and the vertical conductive part.

The average Nusselt number is plotted in Figure 9 vs aspect ratio (A) at different Reynolds number for $\mathrm{Ra} = 1$, which can be thought as the dominating force convection situation. In the figure the dots represent the simulation results with *LBM* and the lines are the analytical solutions. It can be investigated that for each Reynolds number, the present proposed solution (combining equations (18)-(20)) expressed as

$$\mathrm{Nu} = 0.254 \times \mathrm{Re}^{0.47} \times \mathrm{A}^{1/2} + (\mathrm{A} - 1) \tag{21}$$

The agreement is good between the numerical results and the proposed scale analytical expression. The obtained equation (20) is not useful for low Re and low A

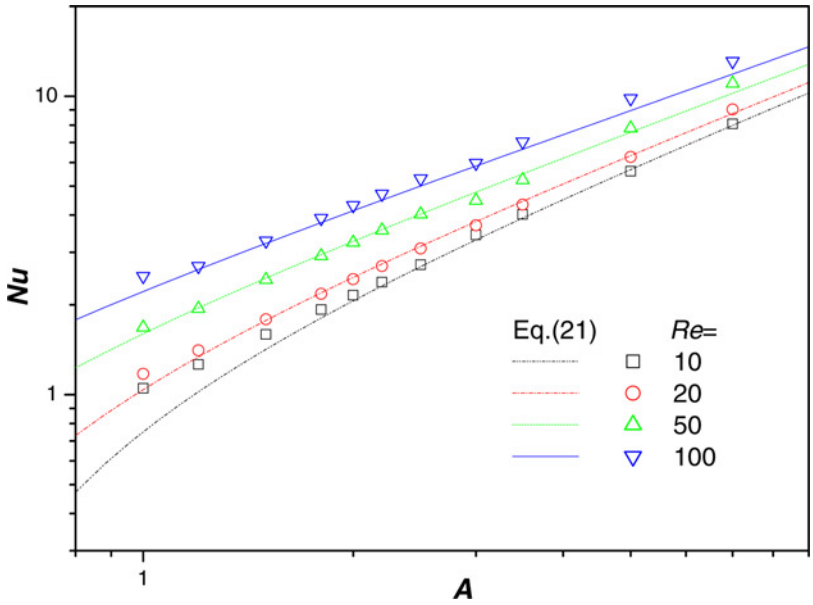

Figure 9.
Average Nusselt number versus aspect ratio, A, and different Re

because the convective part is not significant and the transfer tends to the conductive part, such discrepancy is obvious in Figure 9 for Re = 10 and low A. We underline also the second limitation of the obtained expression (equation (21)) for the high Re and A due to the strong secondary recirculating cell (*C2*) inducing a convective transfer contribution on the conductive domain, for example, when aspect ratio is large in Figure 7 (A = 5), in the upper part of the rectangular, the local Nusselt number changes with height in monotone for several times, which reveals that there are series of vortices. Such effect induces an increase of the heat transfer and the expression underestimate the Nu as represented in Figure 9 for Re = 100 and A > 5.

In Table II, the average Nusselt numbers based on the simulation solution and on the analytical solution are compared for different aspect ratios when Ra = 1 and Re = 50. It reveals that the analytical formula (21) could be applied to evaluate the average Nusselt number when the mixed flow is dominated by forced convection at low Reynolds numbers where the relative error remain less than 4 percent, except for the Re = 100 and A $\geq$ 2 where error increase (such limitation was underlined in the previous section).

The coupled problem is now mastered in case of mixed convection by using the Ri number and we found an expression based on scale analysis to take into account the aspect ratio in case of dominating forced convection. We are working to generalize such results in order to fill on the entire mixed convection domain and also identify an accurate expression (conditions) illustrating the condition of using such expression.

4. Conclusion

The lattice Boltzmann moment model is applied to simulate mixed flow in a vertical rectangular cavity. The effects of Rayleigh number and Reynolds number on heat transfer and flow fluid are performed by Richardson number. The aspect ratio effects on flow and heat transfer are investigated. In view of the results, the following findings are summarized. The case of dominated forced convection exhibit a upper convective cell of square shape inducing a main convective domain decreasing with the increases of A.

- The mixed flow in slender rectangular exhibits a competition between natural and forced convection. The main flow and heat transfer characteristics are compared when Rayleigh number and Reynolds number change.
- For a fixed aspect ratio, the governing parameter, Richardson number, is defined to identify which flow is dominating as $Ri = Ra/Pr \times Re^2$. For Ri much smaller than unity, the flow and heat transfer is dominated by forced convection and the average Nusselt number only changes with Reynolds number. For Ri much

	Re = 20		50		100	
A	Simulation	Analytical (relative error, %)	Simulation	Analytical (relative error, %)	Simulation	Analytical (relative error, %)
1.5	1.7899	1.7716 (1.02)	2.4285	2.4561 (1.14)	3.2769	3.2094 (2.06)
2.0	2.4389	2.4683 (1.21)	3.2367	3.2587 (0.68)	4.3080	4.1286 (4.16)
2.5	3.0900	3.1416 (1.67)	4.0259	4.0253 (0.01)	5.2944	4.9979 (5.60)
3.0	3.6958	3.7983 (2.77)	4.5962	4.7663 (3.70)	5.9715	6.8317 (3.34)
5.0	6.2600	6.3217 (0.99)	7.8146	7.5713 (3.11)	9.8303	8.9467 (8.99)

Table II.
Comparison of the average Nusselt numbers of simulation and of analytical formulae

larger than unity, it is dominated by natural convection and the average Nusselt number only changes with Rayleigh number. For Ri is order of unity, it is a mixed regime and the average Nusselt number is affected by both Reynolds number and Rayleigh number.

- When the flow and heat transfer is dominated by forced convection, an analytical expression based on scale analysis is obtained to evaluate the effect of aspect ratio on the average Nusselt number. It is composed of convection and conduction contributions and expressed as: $\mathrm{Nu} = \mathrm{Nu}_{\mathrm{cv}} \times 1/\ \ \mathrm{A} + \mathrm{Nu}_{\mathrm{cd}} \times (1 - 1/\mathrm{A})$ combined the expressions of convection and conduction, it can be expressed as $\mathrm{Nu} = 0.254 \times \mathrm{Re}^{0.47} \times \mathrm{A}^{1/2} + (\mathrm{A} - 1)$. A good agreement is obtained between the analytical solution and simulation results with *LBM* within the scope of present study.

References

Alexander, F., Chen, S. and Sterling, J.D. (1993), "Lattice Boltzmann thermo-hydrodynamics", *Physical Review E*, Vol. 47, p. R2249.

Ameziani, D.E., Guo, Y., Bennacer, R., El Ganaoui, M. and Bouzidi, M. (2008), "Competition between Lid driven and natural convection in square cavity: lattice Boltzmann method", *Proceedings of the CHT 08, Marrakech-Maroc*, *11-16 Mai 2008*, available at: www.begellhouse.com

Chen, Y., Ohashi, H. and Akiyama, M. (1994), "Thermal lattice Bhatatnagar-Gross-Krook model without nonlinear deviations in macrodynamic equations", *Physical Review E*, Vol. 50 No. 4. pp. 2776-83.

Cheng, M. and Hung, K.C. (2006), "Vortex structure of steady flow in a rectangular cavity", *Computers & Fluids*, Vol. 35, pp. 1046-62.

Chew, Y.T., Shu, C. and Niu, X.D. (2002), "A new differential lattice equation and its application to simulate incompressible non-uniform grids", *Journal of Statistical Physics*, Vol. 107 No. 112, p. 329.

Choukairy, K., Bennacer, R. and Vasseur, P. (2004), "Natural convection in a vertical annulus boarded by an inner wall of finite thickness", *International Communications in Heat and Mass Transfer*, Vol. 31 No. 4, pp. 501-12.

De Vahl Davis, G. and Jones, I.P. (1983), "Natural convection in a square cavity: a comparison exercise", *International Journal for Numerical Methods in Fluids*, Vol. 3 No. 3, pp. 227-48.

d'Humieres, D. (1992), "Generalized lattice-Boltzmann equations, rarefied gas dynamics: theory and simulations", in Shizgal, B.D. and Weaver, D.P. (Eds), *Progress in Astronautics and Aeronautics*, AIAA, Washington, DC, Vol. 159.

Ghia, U., Ghia, K.N. and Shin, C.T. (1982), "High-resolutions for incompressible flow using Navier-Stokes equations and a multigrid method", *Journal of Computational Physics*, Vol. 48, p. 387.

Guo, Z., Shi, B. and Wang, N. (2000), "Lattice BGK model for incompressible Navier–Stokes equation", *Journal of Computational Physics*, Vol. 165, p. 288.

Haibo Huang, T.S., Lee, C. and Shu, (2007), "Lattice Boltzmann method simulation gas slip flow in long microtubes", *International Journal of Numerical Methods for Heat and Fluid Flow*, Vol. 17 No. 6, pp. 587-607.

He, X.Y., Chen, S.Y. and Doolen, G.D. (1998), "A novel thermal model for the lattice Boltzmann in incompressible limit", *Journal of Computational Physics*, Vol. 146 No. 1, pp. 282-300.

Heijs, A.W.J. and Lowe, C.P. (1995), "Numerical evaluation of the permeability and the Kozeny constant for two types of porous media", *Physical Review E*, Vol. 51, p. 4346.

Hou, S., Zou, Q., Chen, S., Doolen, G. and Cogley, A.C. (1995), "Simulation of cavity flow by the lattice Boltzmann method", *Journal of Computational Physics*, Vol. 118, p. 329.

Iwahara, D., Shinto, H., Miyahara, M. and Higashitani, K. (2003), "Liquid drops on homogeneous and chemically heterogeneous surfaces: a two-dimensional lattice Boltzmann study", *Langmuir*, Vol. 19, p. 9086.

Ladd, A.J.C. (1994), "Numerical simulations of particulate suspensions via a discretized Boltzmann equation, part 1-2. Theoretical foundation", *Journal of Fluid Mechanics*, Vol. 271, p. 285.

Mezrhab, A., Bouzidi, M. and Lallemand, P. (2004), "Hybrid lattice-Boltzmann finite-difference simulation of convective flows", *Computers & Fluids*, Vol. 33, pp. 623-41.

Mezrhab, A., Jami, M., Bouzidi, M. and Lallemand, P. (2007), "Analysis of radiation–natural convection in a divided enclosure using the lattice Boltzmann method", *Computers & Fluids*, Vol. 36, pp. 423-34.

McNamara, G. and Alder, B. (1993), "Analysis of the lattice Boltzmann treatment of hydrodynamics", *Physics A*, Vol. 194 Nos. 1/4, pp. 218-28.

Palmer, B.J. and Rector, D.R. (2000), "Lattice-Boltzmann algorithm for simulating thermal two-phase flow", *Physical Review E*, Vol. 61 No. 5, p. 5295.

Patil, D.V., Lakshmisha, K.N. and Rogg, B. (2006), "Lattice Boltzmann simulation of lid-driven flow in deep cavities", *Computers & Fluids*, Vol. 35, pp. 1116-25.

Raiskinmäki, P., Koponen, A., Merikoski, J. and Timonen, J. (2000), "Spreading dynamics of three-dimensional droplets by the lattice-Boltzmann method", *Computational Materials Science*, Vol. 18, p. 7.

Sai, B.V.K.S., Seetharamu, K.N. and Narayana, P.A.A. (1994), "Solution of transient laminar natural convection in a square cavity by an explicit finite element scheme", *Numerical Heat Transfer, Part A*, Vol. 25, pp. 593-609.

Semma, E., El Ganaoui, M., Bennacer, R. and Mohamad, A.A. (2008), "Investigation of flows in solidification by using the lattice Boltzmann method", *The International Journal of Thermal Sciences*, Vol. 47 No. 3, pp. 201-8.

Shan, X. and Doolen, G. (1995), "Multicomponent lattice-Boltzmann model with interparticle interaction", *Journal of Statistical Physics*, Vol. 81, p. 379.

Shankar, P.N. and Deshpade, M.D. (2000), "Fluid mechanics in the driven cavity", *Annual Review of Fluid Mechanics*, Vol. 32, pp. 337-52.

Succi, S., Foti, E. and Higuera, F. (1989), "Simulation of three-dimensional porous media with the lattice Boltzmann method", *Europhysics Letters*, Vol. 10 No. 5, p. 433.

Suppa, D., Kuksenok, O., Balazs, A.C. and Yeomans, J.M. (2002), "Phase separation of a binary fluid in the presence of immobile particles: a lattice Boltzmann approach", *Journal of Chemical Physics*, Vol. 116 No. 14, p. 6305.

Tang, G.H., Tao, W.Q. and He, Y.L. (2003), "Simulation of fluid flow and heat transfer in a plane channel using the lattice Boltzmann method", *International Journal of Modern Physics B*, Vol. 17 Nos. 1/2, p. 183.

Tekitek, M.M., Bouzidi, M., Dubois, F. and Lallemand, P. (2006), "Adjoint lattice Boltzmann equation for parameter identification", *Computers & Fluids*, Vol. 35, pp. 805-13.

Vladimirova, N., Malagoli, A. and Mauri, R. (1999), "Two-dimensional model of phase segregation in liquid binary mixtures", *Physical Review E*, Vol. 60, p. 6968.

Wong, J.C.-F. (2007), "Numerical simulation of two-dimensional laminar mixed-convection in a lid-driven cavity using the mixed finite element consistent splitting

scheme", *International Journal of Numerical Methods for Heat & Fluid Flow*, Vol. 17 No. 1, pp. 46-93.

Xu, A., Gonnella, G. and Lamura, A. (2003), "Phase-separating binary fluids under oscillatory shear", *Physical Review E*, Vol. 67, p. 056105.

Zhang, R. and Chen, H. (2003), "Lattice Boltzmann method for simulations of liquid-vapor thermal flows", *Physical Review E*, Vol. 67, p. 066711.

Corresponding author
Y. Guo can be contacted at: ylguo@dlut.edu.cn